

## ARTICLE

# Scaled concrete beams containing maximum levels of coarse recycled aggregate: Structural verifications for precast-concrete building applications

Francisco Fiol<sup>1</sup>  | Víctor Revilla-Cuesta<sup>2</sup>  | Marta Skaf<sup>1</sup>  |  
 Carlos Thomas<sup>3</sup>  | Juan M. Manso<sup>2</sup> 

<sup>1</sup>Department of Construction, Escuela Politécnica Superior, University of Burgos, Burgos, Spain

<sup>2</sup>Department of Civil Engineering, Escuela Politécnica Superior, University of Burgos, Burgos, Spain

<sup>3</sup>LADICIM (Laboratory of Materials Science and Engineering), E.T.S. de Ingenieros de Caminos, Canales y Puertos, University of Cantabria, Santander, Spain

## Correspondence

Víctor Revilla-Cuesta. Department of Civil Engineering, Escuela Politécnica Superior, University of Burgos, C/ Villadiego s/n, Burgos 09001, Spain.  
 Email: vrevilla@ubu.es

## Funding information

Agencia Estatal de Investigación; European Commission; European Regional Development Fund; Junta de Castilla y León; Ministerio de Ciencia e Innovación; Universidad de Burgos

## Abstract

The use of Recycled aggregate (RA) enhances concrete sustainability. If used on an industrial-scale, structural verification, and testing will be required to confirm that RA concrete can meet relevant industrial standards and the requirements of manufacturers, especially in the precast-concrete industry. In this paper, an experimental campaign with the participation of a precast-concrete manufacturer is reported. The objective is to test a self-compacting concrete (SCC) mix, designed for structural applications, that contains maximum amounts of 100% coarse RA, in order to establish its compliance with the habitual requirements of precast-concrete manufacturers. Thus, scaled beams (12 × 24 × 180 and 24 × 24 × 130 cm) were subjected to bending, shear-bending, shear, and long-term-deflection tests. In addition, the performance of that SCC mix in the bending and shear-bending tests was compared with the performance of an SCC mix of similar compressive strength containing 0% coarse RA. In the failure tests, the experimental results were between 1.5 and 3 times higher than the required values. The elastic behavior of both SCC mixes was also very similar in those tests, regardless of the amount of coarse RA, due to the robust design of the water and superplasticizer content of the SCC, which balanced the decreased flowability and the lower compressive strength of SCC that resulted from the additions of coarse RA. The SCC mix with 100% RA showed a lower load-bearing capacity after failure and narrow compliance margins with the deflection limits of the long-term-deflection test. Even though the SCC mix with 100% RA met all the standard technical specifications of the precast-concrete manufacturer, reference should always be made to the serviceability limit states that are applicable at the time of the structural design phase.

**Acronyms:** NA, Natural aggregate; RA, Recycled aggregate; SCC, Self-compacting concrete.

This is an open access article under the terms of the [Creative Commons Attribution-NonCommercial-NoDerivs](https://creativecommons.org/licenses/by-nc-nd/4.0/) License, which permits use and distribution in any medium, provided the original work is properly cited, the use is non-commercial and no modifications or adaptations are made.

© 2023 The Authors. *Structural Concrete* published by John Wiley & Sons Ltd on behalf of International Federation for Structural Concrete.

**KEYWORDS**

bending test, long-term deflection test, precast-concrete-application trials, recycled aggregate self-compacting concrete, shear test, shear-bending test

## 1 | INTRODUCTION

The manufacture of conventional raw materials for concrete production entails environmental impacts that are now quite well known. On the one hand, the extraction of natural aggregate (NA) from quarries and gravel pits<sup>1</sup> changes the geographic contours of the terrain, vegetative cover, and even water courses, causing secondary environmental impacts.<sup>2</sup> On the other hand, cement manufacturing produces significant CO<sub>2</sub> emissions. It is estimated that there are 0.8 tons of atmospheric emissions of CO<sub>2</sub> for every ton of cement that is produced, accentuating global warming and climate change.<sup>3</sup> In view of this situation, the production of concrete with sustainable raw materials, generally industrial by-products, has been addressed in numerous research projects. Their aims are to recover materials that might otherwise go unused, in addition to mitigating the above-mentioned environmental impacts and curtailing illegal dumping at landfill sites.<sup>4,5</sup> Those sustainable raw materials have included “green” binders, such as fly ash,<sup>6</sup> ground granulated blast furnace slag,<sup>7</sup> and silica fume,<sup>8</sup> in substitution of ordinary Portland cement, and alternative aggregates, such as electric arc furnace slag,<sup>9</sup> and rubber,<sup>10</sup> as well as recycled aggregate (RA)<sup>11</sup> in substitution of NA. The focus of this study is on the use of RA.

RA is probably the most widely studied sustainable aggregate in the literature.<sup>12,13</sup> Although all RA is sourced from the crushing of unused concrete components,<sup>14,15</sup> a distinction is usually drawn between the behavior of the coarse and the fine fractions:

- The coarse fraction is composed of particles >4 mm that consist of NA and adhered mortar.<sup>16,17</sup> Compared to coarse NA, the presence of adhered mortar in coarse RA lowers its density, raises its water absorption levels, and lessens its adherence within the new cementitious concrete matrix when used as an aggregate.<sup>18,19</sup> All these aspects decrease concrete workability, strength, and elastic stiffness.<sup>20</sup> However, if the water-to-cement ratio is reduced, both the in-fresh and the mechanical behavior are impaired whenever coarse RA is added; effects that the use of RA from the crushing of high-strength concrete can accentuate.<sup>21,22</sup>
- The fine fraction of RA consists of particles <4 mm. The most relevant aspect is in its smaller particles <0.5 mm,<sup>23</sup> as the characteristics of its larger particles

and the particles of the coarse RA fraction are similar. The 0/0.5 mm fraction of fine RA is characterized by a high content of mortar and unhydrated cement particles.<sup>24</sup> These particles, apart from lowering its density, mean that fine RA can absorb 7–8 times more water than fine NA,<sup>25</sup> lowering the quality of the cementitious matrix of the new concrete, and greatly increasing its porosity.<sup>26</sup> Additions of fine RA can therefore notably decrease both the mechanical properties and the durability of the concrete product.<sup>27</sup> Modifying the composition of concrete to find a solution to these problems is at best complicated. Hence, the importance of a precise quantification of the right quantity of fine RA, above which concrete performance will deteriorate.<sup>28</sup>

Structural verification is a fundamental step to ensure that an alternative concrete composition can be used in structural components for building and civil-engineering projects.<sup>29</sup> Hence the abundant literature on the structural verification of concretes containing sustainable raw materials,<sup>30,31</sup> including RA<sup>32</sup>:

- In a first stage, studies were conducted on adhesion between concrete and steel reinforcements, a fundamental aspect for the optimum performance of reinforced concrete.<sup>33,34</sup> The use of RA was found to reduce adhesion,<sup>35</sup> although better RA quality to some extent countered that negative effect.<sup>36</sup> Moreover, the addition of fibers was found to improve RA-concrete bonding in one study.<sup>37</sup> In another study,<sup>38</sup> the bond-design equations specified in certain standards were calibrated through reliability-based analyses.
- Secondly, the behavior of full-scale beams was studied. It was found that the difference in the failure load between beams containing coarse-RA concrete and their NA-concrete counterparts was higher under bending stresses than under shear loads.<sup>39</sup> Moreover, coarse-RA concrete also led to increased deflections under service conditions.<sup>40</sup> The addition of fine RA further worsened the performance of the beams when it was incorporated in concrete.<sup>41</sup> In principle, the strength capacity values that are estimated in current standards are on the safe side,<sup>39,42</sup> although the models were extensively tested in various studies, to ensure the reliability of the calculation methods. Thus, partial factors to offset the effects of using RA on beam-design

safety have been proposed.<sup>43,44</sup> The same aspects have also been analyzed in full-scale columns.<sup>32,45</sup>

- Finally, improvements to the structural behavior of beams and columns made with RA concrete were also addressed in another studies.<sup>46</sup> The confinement of RA concrete in columns and the reinforcement of RA-concrete beams with jackets and textile composites were found to improve performance.<sup>47,48</sup> These techniques show that the ductile behavior of concrete improves with the addition of RA<sup>48</sup> and that the repair of damaged RA concrete structures is both feasible and safe.<sup>47</sup>

In view of the above research framework, the next step in the investigation of RA concrete will be to evaluate whether this type of concrete can be used in structural applications on an industrial scale. The precast-concrete industry is currently expanding, as precast-concrete elements are used with greater frequency in both buildings and civil works.<sup>49</sup> Moreover, faulty concrete components can be crushed to produce RA aggregate at almost any precast-concrete plant.<sup>50</sup> Therefore, an assessment of whether RA concrete meets the specifications that are commonly required in the precast-concrete industry will represent a step forward for the application of RA concrete on an industrial scale. However, it must be considered that self-compacting concrete (SCC) is used in the precast-concrete industry, as this type of concrete increases output, due to its high flowability, with no need for concrete vibration, which saves both time and energy costs,<sup>51</sup> as well as guaranteeing adequate concreting of heavily reinforced elements.<sup>52</sup> According to the current literature, the use of RA for SCC production is also quite feasible, provided a careful design phase is followed to achieve the high levels of workability that characterize SCC, whilst at the same time ensuring that the amount of RA is not excessive and will not result in any loss of concrete strength.<sup>53</sup>

In this paper, an experimental test campaign was conducted of SCC beams containing 100% coarse RA, as part of the structural verification of this concrete in precast-concrete building applications. A previously existing procedure developed at a local precast-concrete company was followed that the company habitually employs for the validation of the concrete mixes used to manufacture its building products. Thus, scaled beams were produced and manufactured at the precast-concrete plant and were subsequently tested at the structural materials laboratory that the company uses. In a first stage, two SCC mixes were designed and produced with 0% and 100% coarse RA, respectively, which were subjected to bending and shear-bending tests. In a second stage, scaled beams made with the mix containing 100% coarse RA were

subjected to shear and long-term-deflection tests. In all cases, the scaled beams made with 100% coarse RA met the requirements of the precast-concrete company that participated in this research project, suggesting that the beams could be used in precast-concrete building applications, although a serviceability-based design is always recommended.

## 2 | DESIGN AND CHARACTERIZATION OF SCC MIXES

In this section, the design and both the fresh and the mechanical properties of the SCC mixes used to produce the beams for structural testing are described.

### 2.1 | Raw materials

The raw materials used to prepare the SCC mixes were supplied from the precast-concrete company that had agreed to participate in this research. The company employs these materials to produce the concrete mixes for its precast-concrete components.

Two SCC mixes were prepared which incorporated CEM I 52.5 R (EN 197-1<sup>54</sup>), with a density of approximately 3.12 Mg/m<sup>3</sup>; drinking water from the mains supply, containing no compounds that could be detrimental to concrete mixes; two superplasticizers, necessary to achieve high levels of self-compactability without increasing the water-to-cement ratio to a level that could cause a large decrease in strength<sup>21</sup>; and limestone filler <0.063 mm, with a density of 2.77 Mg/m<sup>3</sup>, and a purity of 96.5%, which improved the filling capacity and strength performance of SCC.

The precast-concrete company usually extracts its own NA from a company gravel pit that is supplied in the form of a siliceous aggregate of rounded shape in two fractions, 0/2 and 2/12.5 mm. The RA was produced from precast-concrete beams and columns manufactured at the precast company plant with compressive strengths higher than 45 MPa that had been rejected due to faulty sizes or geometrical defects. Thus, the parent concrete of the RA could be considered of a high quality.<sup>55</sup> Company machinery was used to produce the RA, by means of hydraulic clamping, followed by jaw and impact crushing. Finally, sieving produced a coarse RA 4/12.5 mm. No use was made of fine RA in this study. Figure 1 shows the particle sizes of the above-mentioned aggregates, while Table 1 shows the higher water absorption and lower density of coarse RA compared to NA.

## 2.2 | Mix design

Two SCC mixes were formulated with 0% (mix *C*) and 100% (mix *CR*) coarse RA, respectively, whose composition is shown in Table 2. Mix *CR* was designed, because the goal of the experimental campaign was to verify whether a mix with large amounts of coarse RA met the requirements for the production of precast-concrete building components at a precast-concrete plant continually engaged in the production of these sorts of products. However, a comparison of the bending and shear-bending test behaviors of that mix and a mix with 100% coarse NA was considered worthwhile, in order to analyze the effects of coarse RA additions. Mix *C* was therefore also developed.

First, mix *C* (0% coarse RA) was designed. This mix was proportioned to meet the fresh and hardened performance specifications that are required at the company plant: a slump class SF1 (slump flow of  $600 \pm 50$  mm) or higher according to EN 206<sup>54</sup>; a viscosity-slump-flow class of at least VS2 ( $t_{500}$  between 2 and 5 s) according to

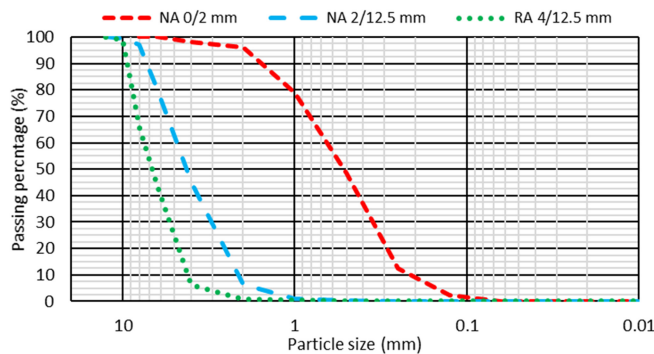


FIGURE 1 Particle size of the aggregates (EN 933-1<sup>54</sup>).

TABLE 1 Density and water absorption levels of the aggregates (EN 1097-6<sup>54</sup>).

Property	Saturated-surface-dry density (Mg/m <sup>3</sup> )	24-h water absorption (%)
NA 0/2 mm	2.64	0.26
NA 2/12.5 mm	2.63	1.16
RA 4/12.5 mm	2.41	4.15

TABLE 2 Mix design (kg/m<sup>3</sup>).

Mix	CEM I		Admixture 1	Admixture 2	Limestone filler	NA 0/2 mm	NA 2/12.5 mm	RA 4/12.5 mm
	52.5 R	Water						
<i>C</i>	320	112	0.55	1.32	280	650	1150	0
<i>CR</i>	320	112	0.90	2.20	280	720	0	1040

EN 206<sup>54</sup>; and a minimum compressive strength of 45 MPa according to EN 12390-3.<sup>54</sup> The initial proportions of the components of this mix were defined according to the usual industrial dosage of SCC, although they were subsequently empirically modified to meet those requirements.

Afterwards, mix *CR* was designed. To do so, 100% coarse NA was replaced with RA using the volume correction method. In addition, as the coarse NA 2/12.5 mm was replaced with coarse RA 4/12.5 mm, due to the desire to limit this research to the coarse fraction of RA, the content of NA 0/2 mm was also increased when adding RA, to adjust the particle size of the mix. Finally, the water content was not increased to compensate for the higher water absorption levels of coarse RA, thus offsetting the expected decrease in strength following the additions of coarse RA.<sup>21</sup> However, no increase in water content decreased SCC flowability, which was partially solved by increasing the plasticizing-admixture content. In this way, mix *CR* also met the in-fresh and in-hard behavioral specifications of the precast-concrete company, which were identical to those established for mix *C*.

## 2.3 | SCC production

The SCC mixes were produced on an industrial scale. Both mixes were manufactured at the precast-concrete plant in volumes of 2 m<sup>3</sup> in a vertical-axis concrete mixer. Other plant facilities (storage hoppers, raw-material weighing systems, etc.) were also used. A two-stage mixing process was followed, in order to achieve adequate flowability:

- The first stage of mixing consisted of wetting the concrete mixer. Subsequently, the coarse and fine aggregate and the first half of the water were progressively added and mixing continued for another 3 min, to assist aggregate water absorption, so that the flowability of the SCC remained constant.<sup>56</sup>
- The second stage consisted of adding the remaining raw materials: cement, limestone filler, admixtures, and the second half of the water. After that, the SCC was mixed for 5 min to ensure optimal aggregate water absorption, and adequate cement hydration.<sup>57</sup>

## 2.4 | Fresh and mechanical properties of SCC mixes

After mixing, a concrete sample was taken to perform the slump-flow test (EN 12350-8<sup>54</sup>), and the specimens for the mechanical characterization of the mixes were prepared. For each SCC mix, fifteen 15 × 30-cm cylindrical specimens were prepared to measure the compressive strength (EN 12390-3<sup>54</sup>) at 1, 7, 28, and 180 days and the splitting tensile strength (EN 12390-6<sup>54</sup>) at 28 days. Each property was determined on three specimens at each age. All specimens were air cured in the indoor laboratory environment, to simulate the curing of the beams. Table 3 lists both the fresh and the mechanical properties of the mixes:

- Both mixes complied with the SCC flowability requirements at the precast-concrete plant, as indicated in the mix-design section. The addition of coarse RA led to a decrease in SCC flowability that was, on the one hand, due to its high water absorption levels<sup>24</sup> and, on the other, to its irregular shape that hindered the dragging of the aggregate particles within the cement paste.<sup>20</sup> However, these aspects were partially compensated by increasing the amount of plasticizing admixtures.
- Regarding mechanical behavior, the difference in compressive strength between both mixes was minimal, with mix CR even showing a higher strength than mix C at 180 days (62.4 vs. 59.9 MPa). A behavior made possible due to the non-modification of the water content when adding coarse RA, which balanced the expected decrease in strength,<sup>21</sup> as well as due to the good mechanical strength of the parent concrete.<sup>55</sup> Both mixes were designed to have practically identical compressive strengths, so the structural-feasibility analysis was focused on the aggregate type and not on the compressive strength of SCC.
- The mix-design strategy was not as effective in relation to splitting tensile strength, although the difference between the two mixes remained small (less than 5%).

TABLE 3 Fresh and mechanical properties of the SCC mixes.

Property	Mix C	Mix CR
Slump flow (mm)	765 ± 10	680 ± 15
Slump-flow viscosity, $t_{500}$ (s)	2.5 ± 0.2	4 ± 0.1
1-day compressive strength (MPa)	31.1 ± 1.3	32.8 ± 0.4
7-day compressive strength (MPa)	59.1 ± 1.1	56.9 ± 1.3
28-day compressive strength (MPa)	59.4 ± 1.4	58.3 ± 0.9
180-day compressive strength (MPa)	59.9 ± 1.2	62.4 ± 0.7
28-day splitting tensile strength (MPa)	5.5 ± 0.2	5.2 ± 0.1

This could be due to the greater dependence of splitting tensile strength on the bond between the aggregate and the cementitious matrix, which decreased when coarse RA was used.<sup>18</sup> It is also worth noting the greater dispersion of failure modes and experimental values commonly shown by splitting tensile strength compared to compressive strength.<sup>58</sup>

## 3 | BEAM TESTING: TEST DESIGN AND THEORETICAL VALUES

At the same time as the specimens for the mechanical characterization of the mixes were produced, the beams for the structural tests were also prepared, which were tested after 1 year of air curing inside the laboratory. All aspects related to the manufacture of the beams, such as their dimensions and reinforcement, as well as the experimental plan, calculations, and structural verifications conducted, were defined according to the specifications of the precast-concrete plant. The collaborating company uses this same procedure to ensure that any novel concrete mix, such as the one analyzed in this study containing recycled aggregate, is suitable for the manufacture of its precast-concrete components.

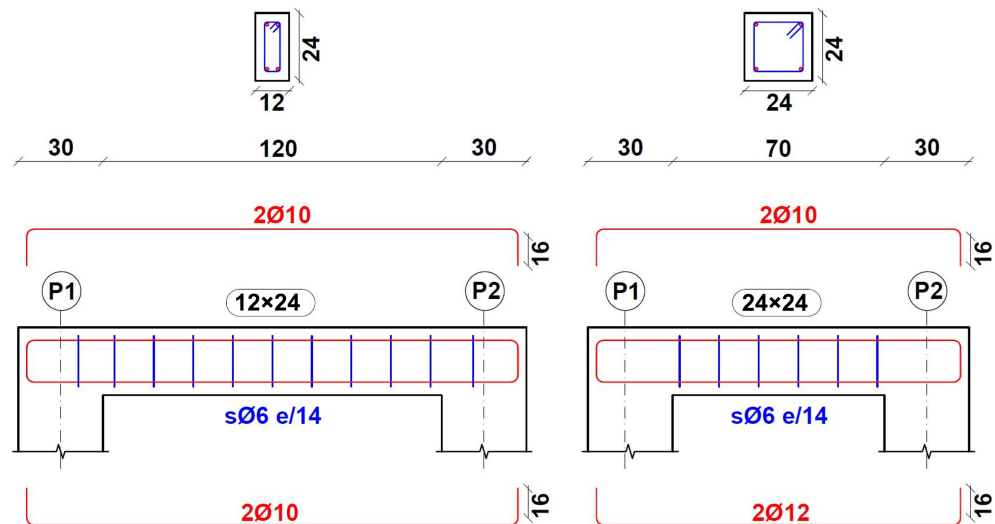
### 3.1 | Rebar characteristics

The scaled reinforced-concrete beams contained 10 and 12 mm diameter rebars for longitudinal tensile reinforcement, 10 mm for the longitudinal compressive reinforcement, and 6 mm for the transverse shear reinforcement. The rebars were the same as those used by the precast-concrete company to reinforce its concrete components: a standardized B 500 SD steel as *per* the specifications of both UNE 36068<sup>59</sup> and Eurocode 2.<sup>60</sup> Following the indications of Eurocode 2,<sup>60</sup> a yield strength of 500 GPa was assumed at a theoretical strain of 4.5‰ for this steel type in the theoretical structural calculations performed. In addition, the plastic field was assumed to cover a strain of up to 10‰.

### 3.2 | Beam details: Dimensions and reinforcement

Both the beam dimensions and the steel reinforcements were the same as the precast-concrete components produced at the company plant, following its established guidelines. Figure 2 depicts a schematic diagram of the beam dimensions and reinforcements.

FIGURE 2 Beam details: dimensions and reinforcement (dimensions in cm).



- Two types of beams were produced for the experimental campaign:  $12 \times 24 \times 180$ -cm beams for bending, shear and long-term-deflection tests; and  $24 \times 24 \times 130$ -cm beams for the shear-bending tests. The test spans were 150 cm (1.5 m) for the bending, shear and long-term-deflection tests, and 100 cm (1.0 m) for the shear-bending test.
- The longitudinal compressive reinforcements consisted of 2010 in all cases. However, the longitudinal tensile reinforcements consisted of 2Ø10 for the  $12 \times 24 \times 180$ -cm beams and 2Ø12 for the  $24 \times 24 \times 130$ -cm beams. For both types of beams, the transverse shear reinforcement consisted of Ø6 stirrups placed every 14 cm. A 15-mm concrete cover was considered for all the reinforcements.

### 3.3 | Beam production

The beams were manufactured at the precast-concrete plant, following the procedure shown in Figure 3. A volume of  $2 \text{ m}^3$  of each SCC was produced in a vertical-axis industrial concrete mixer. Subsequently, the SCC was poured into  $1\text{-m}^3$  concrete skips with automated discharge chutes, through which the beam formworks, previously positioned on the concreting bench, were filled. At the same time as the beams were prepared, the slump-flow test was performed, and the specimens for the mechanical tests were prepared, as detailed in the previous section. Three beams were produced for each test performed on each concrete mix.

### 3.4 | Test set-up

Both bending and shear-bending tests were performed on mixes *C* and *CR*, while the shear and the long-term-

deflection tests were only performed on mix *CR*. The objective was to ascertain whether mix *CR* (100% coarse RA) complied with the necessary specifications that are required for use in precast-concrete components. The same mix was also compared with an SCC mix containing conventional coarse NA in the bending and shear-bending tests.

#### 3.4.1 | Hydraulic actuator

All structural tests, except for the long-term-deflection test, were performed with an MTS model 201.70HF hydraulic actuator with a compressive-loading capacity of 1460 kN and a tensile-loading capacity of 932.5 kN. The built-in load cell was capable of measuring a load of up to 1000 kN at an accuracy of  $\pm 0.01$  kN. In addition, it was equipped with an extensometer for measuring the displacement of the load piston with an accuracy of  $\pm 0.01$  mm. Both magnitudes—applied force and piston displacement—were recorded under a loading rate of 0.05 kN/s, which were the results of the structural tests.

#### 3.4.2 | Bending test

A schematic diagram of the set-up of the scaled beams (dimensions of  $12 \times 24 \times 180$  cm, span of 1.5 m, simply supported beams) during the bending test, in which the load was applied at the midpoint of the test span, is shown in Figure 4a. A photo of the test set-up for the bending test is depicted in Figure 4b.

The load was applied continuously during the test at a rate of 0.05 kN/s, although some stops were made to analyze the cracking of the beams and to mark the cracks

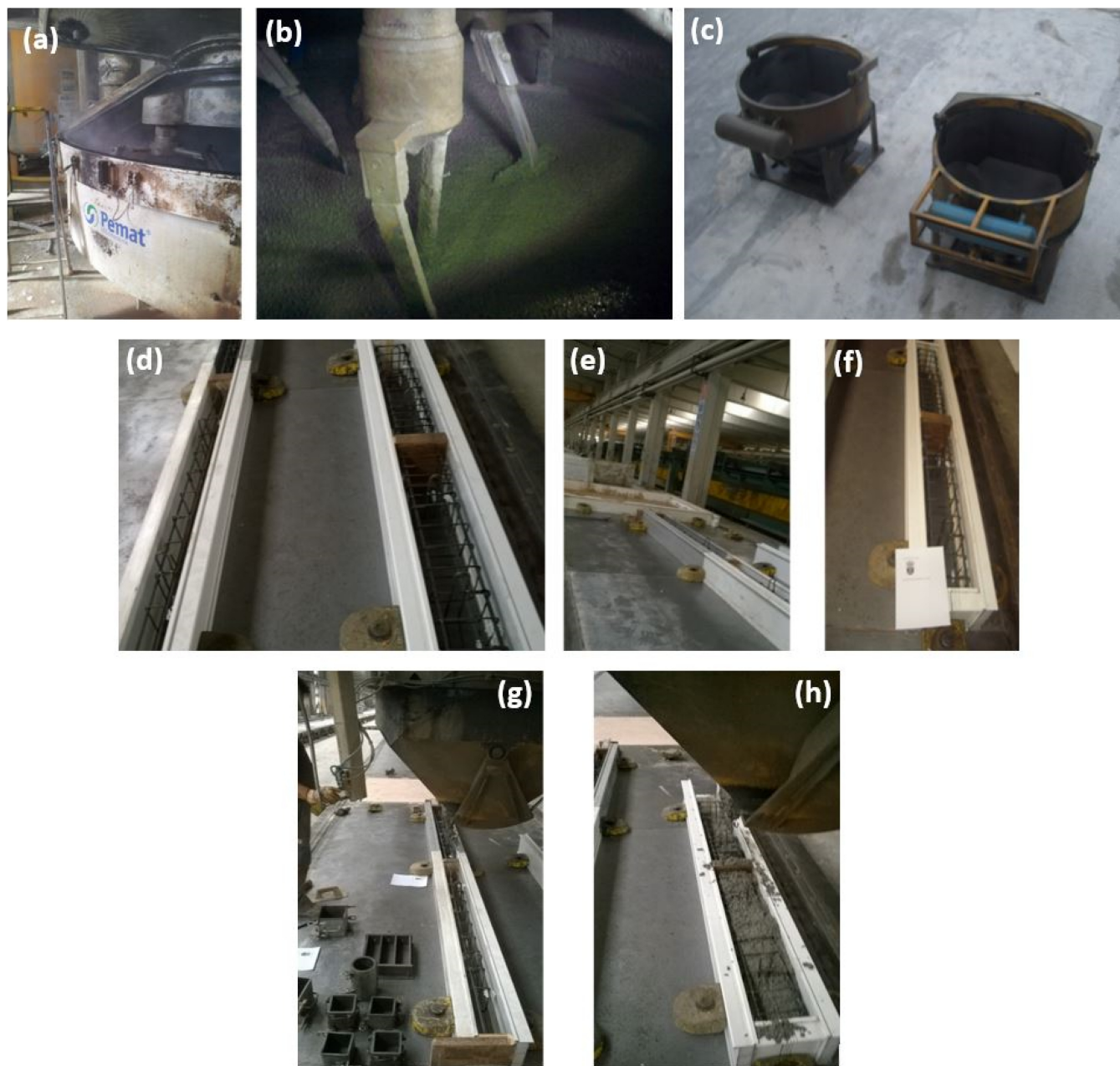


FIGURE 3 Beam production: (a) concrete mixer; (b) concrete mixing; (c) concrete skips; (d–f) beam formworks on the concreting bench; (g) positioning of concrete skip; (h) concrete pouring.

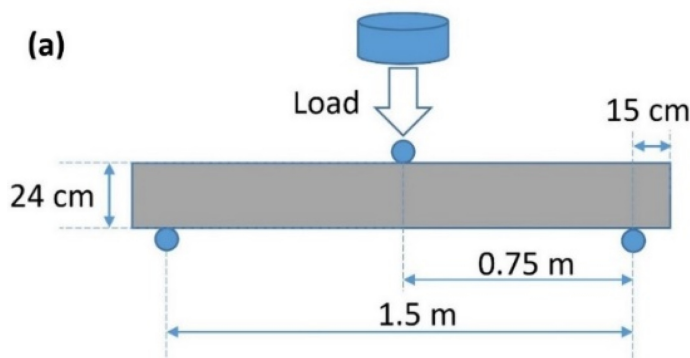
accordingly. As described in the previous section, the use of the actuator enabled the continuous recording of the applied load and piston displacement (beam deflection). Thus, the experimental load-deflection curve was obtained and the experimental values could therefore be compared with the theoretical ones as *per* Eurocode 2.<sup>54</sup> Based on the test results and the theoretical failure stresses, two key structural verifications of the concrete mixes are routine procedure at the precast-concrete company: the bending safety reserve and the bending warning coefficient.

- The bending safety reserve is the percentage difference between the experimental bending-failure moment and the theoretical bending-failure moment as *per* Eurocode 2.<sup>60</sup> It is determined in Equation (1), in which  $BR$  is the bending safety reserve (%);  $LM_{fe}$ , the experimental bending-failure load (kN·m); and  $LM_{ft}$ , the theoretical bending-failure load (kN·m) calculated in accordance with the set-up of the bending test. The minimum bending safety reserve required by the collaborating company is 20%.

FIGURE 4 Bending test:

(a) diagram of test set-up;

(b) photo of test set-up.



$$BR = \frac{LM_{fe} - LM_{ct}}{LM_{fe}} \times 100. \quad (1)$$

- The bending warning coefficient ( $BWC_f$ , dimensionless) refers to the quotient between the experimental bending-failure load ( $LM_{fe}$ , kN·m) and the theoretical bending-cracking load ( $LM_{ct}$ , kN·m) according to the set-up of the test, as shown in Equation (2). The precast-concrete company sets a warning coefficient of 2.5 for all of its concrete mixes.

$$BWC_f = \frac{LM_{fe}}{LM_{ct}}. \quad (2)$$

Furthermore, two other aspects not routinely evaluated at the precast-concrete plant were studied: first, the ratio between the theoretical bending-cracking load and the experimental load when the first crack was detected; second, the bending warning coefficient calculated according to Equation (2), but considering the experimental bending-cracking load. In this way, the feasibility analysis of using SCC with 100% coarse RA under bending stresses could be analyzed with greater accuracy.

### 3.4.3 | Shear-bending test

Based on conventional methods,<sup>60,61</sup> the structural behavior of a beam upon which a point load (or the resulting equivalent load) is applied at the midpoint of its span depends on the quotient between its span and its depth:

- If the quotient is less than two, it is considered to be a “short shear beam.” Under those circumstances, the shear stress will therefore be much greater than the

bending moment, so that the beam will be working exclusively under shear stress and any bending stresses may be disregarded.

- If the quotient is greater than five, it can be considered that the beam almost behaves to an ideally *De Saint Venant beam*.<sup>62,63</sup> Under typical load conditions, the bending stress will be much more relevant than the shear stress, and the beam will experience a bending failure if it incorporates a conventional reinforcement. The load should therefore be applied at a point close to a beam support when a shear test is performed.
- If the quotient is between two and five, it is considered that the beam is simultaneously subjected to bending and shear stresses of the same magnitude and that both stress types to some extent interact. That sort of beams should therefore be subjected to shear-bending tests.

In the shear-bending test, the load was symmetrically applied at the midpoint of the simply supported beam span (Figure 5) at a speed of 0.05 kN/s and with stops to mark the cracking of the beams. Both the applied load and the piston displacement were continuously recorded, so that the bending safety reserve (Equation 1) and the bending warning coefficient (Equation 2) could be evaluated, using the same values habitually employed for the bending tests at the precast-concrete company. However, according to the above-mentioned points, the beams showed a different structural behavior in the shear-bending test (1-m span, 0.24-m height, and 4.17 span-to-height ratio) than in the bending test (1.5-m span, 0.24-m height, and 6.25 span-to-height ratio). Thus, the shear-bending test simulated precast-concrete components subjected to very high loads, but at the same time with a very small span, so that they were simultaneously under high

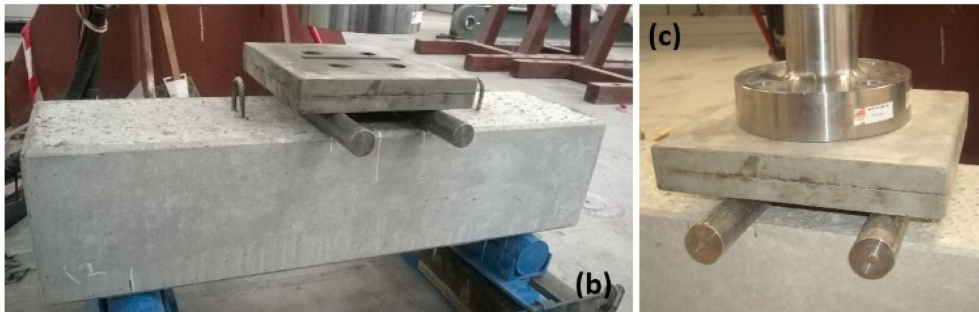
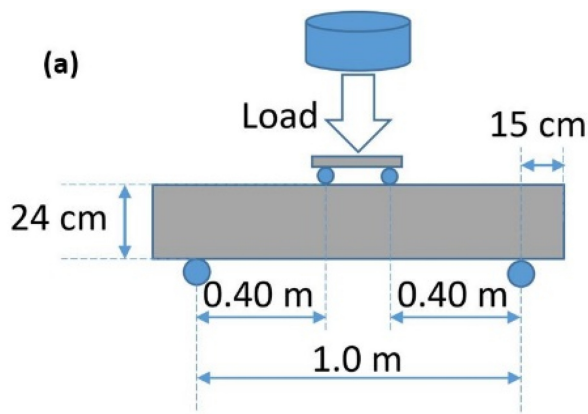


FIGURE 5 Shear-bending test: (a) diagram of test set-up; (b) photo of test set-up; (c) detail of the load-application point.

levels of bending and shear stresses. The precast-concrete company therefore also required a minimum shear safety reserve of 20% in this test, calculated according to Equation (3) (shear safety reserve  $SR$ , %; experimental shear-failure load  $LV_{fe}$ , kN or N; theoretical shear-failure load  $LV_{ft}$ , kN or N, estimated as per Eurocode 2<sup>60</sup> and the set-up of the shear-bending test).

$$SR = \frac{LV_{fe} - LV_{ft}}{LV_{fe}} \times 100. \quad (3)$$

### 3.4.4 | Shear test

The shear test was conducted on simply supported beams of  $12 \times 24 \times 150$  cm, with a span of 1.5 m, as detailed in Figure 6. The load was applied at a point whose distance from the support axis was half of the beam's height, so that the beam was subjected to the highest possible shear. As with the bending and shear-bending tests, the load was applied at a speed of 0.05 kN/s, continuously recording the applied force and the displacement of the piston, although stoppages took place to mark the cracking of the beams. In this test, the only set requirement of the precast-concrete company was a shear safety reserve (Equation 3) of more than 20%, in line with the shear-bending test. Nevertheless, the shear safety reserve regarding the cracking point was also evaluated.

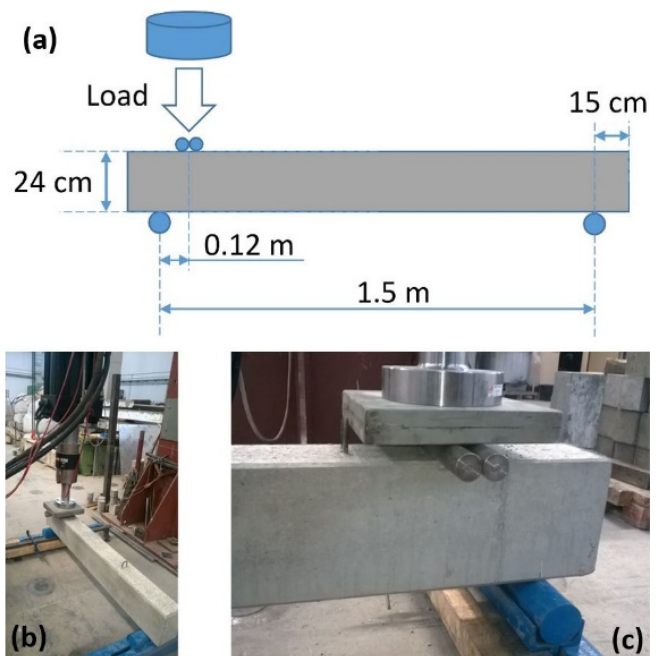


FIGURE 6 Shear test: (a) diagram of test set-up; (b) photo of beam test set-up; (c) detail of the load-application point.

### 3.4.5 | Long-term-deflection test

The long-term-deflection test consisted of applying a point load at the center point of the test beams for 364 days. It was not considered feasible to use the actuator employed in the other tests, as only one actuator was

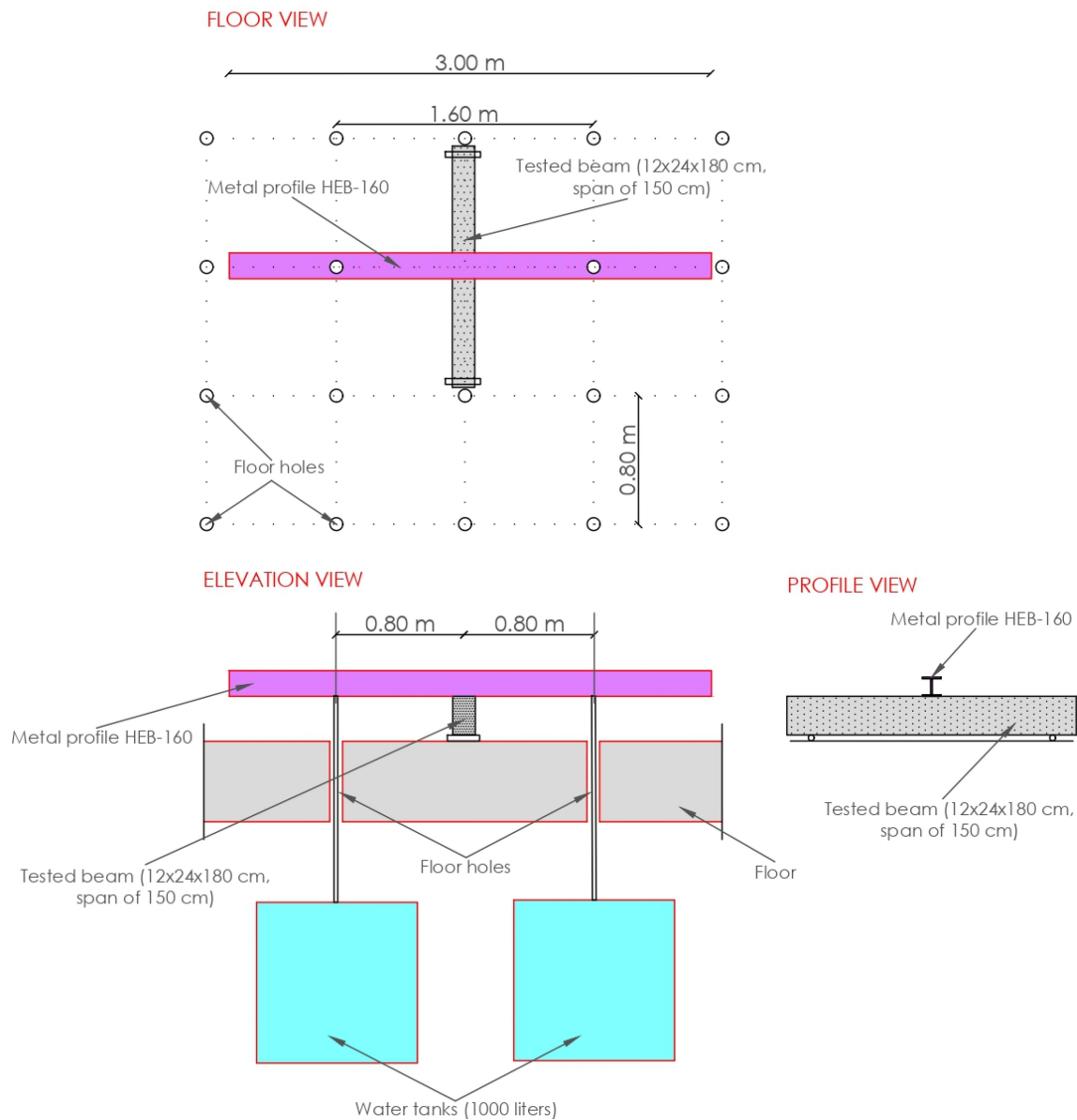


FIGURE 7 Set-up of the long-term-deflection test.

available and it was necessary to simultaneously test three beams, hence the test set-up is shown in Figure 7. The  $12 \times 24 \times 180$ -cm beams (test span of 150 cm) were simply supported and an HEB-160 steel profile (EN 10034<sup>54</sup>) was supported perpendicular to the beam at its midpoint. Two 1000-liter water tanks were hung from each end of the steel profile. In this way, the weight of the water was transferred to the steel profile and from there to the midpoint of the beam. As the steel profile was simply supported on the beam (with no continuity) and the arrangement of the tanks was symmetrical, only a point load and no bending moment were transmitted to the concrete beam. The slabbed floor of the laboratory where the experimental campaign was performed, with a basement and a mesh of small 0.80 x 0.80 m holes for the anchorage of

different types of frames and actuators, proved useful for suspending the water tanks from the steel profile. Figure 8 illustrates the experimental set-up for one of the beams. The test set-up was maintained in place for 364 days, thus subjecting the beams to long-term loading. The deflections of the beams over this period of time were continuously measured using an LVDT located at the midpoint of each beam and were compared with the theoretical deflections. The precast-concrete company participating in the research requested that the instant and long-term (after 364 days) deflections be no higher than 80% and 55% of the theoretical values, respectively.

The choices of both water-tank capacity (1000 liters) and the type of steel profile in use (HEB 160) were jointly decided in consultation with the precast-concrete

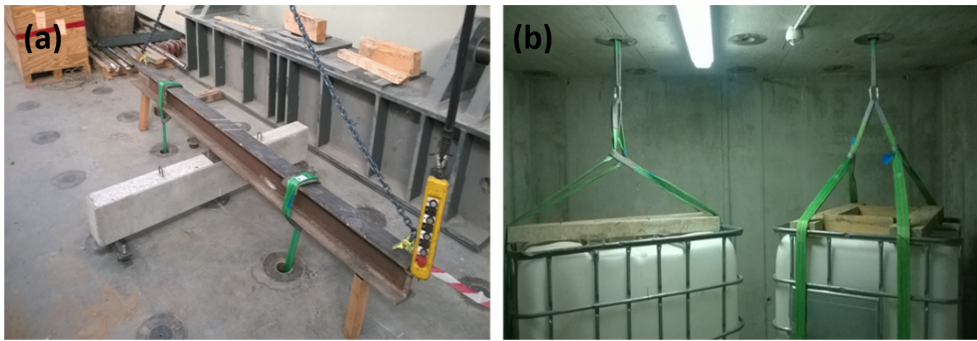


FIGURE 8 Long-term-deflection test: (a) real arrangement of a beam; (b) water tanks.

Element	Material	Unit weight	Load (N)
Metal profile HEB-160	Steel	580 N/m	1740
Two water tanks (empty)	Plastic and steel	545 N/tank	1090
Water (inside the tanks)	Water	10,000 N/tank	20,000
Total load	-	-	22,830

TABLE 4 Total point load applied in the long-term-deflection test.

company, thus achieving the required load to be applied. The load applied to the test beams is detailed in Table 4, to which the own weight of each beam, estimated at 705 N/m, was added.

### 3.5 | Theoretical cracking and failure loads

The structural verification in each (bending, shear-bending and shear) failure test involved a comparison between the theoretical cracking and failure loads and the experimental (real) value of the actuator load at the cracking and failure points. Therefore, the theoretical values of the cracking and failure loads were calculated for each type of beam, as shown in Table 5. These calculations were performed following each test set-up (Figures 4a, 5a, and 6a) using software programmed with the standard specifications of Eurocode 2.<sup>60</sup> Thus, both concrete and steel were considered to work in the elastic field and the corresponding unitary safety coefficients were applied. This calculation procedure was chosen because the precast-concrete company, that is located in Spain, applies the Eurocode 2 standard<sup>60</sup> to the design of its reinforced precast-concrete components. The theoretical values of the cracking and failure loads were the same for both SCC mixes, as both were of practically identical compressive strengths (Table 3).

The theoretical long-term-deflection curve was also calculated for the long-term-deflection test following the standard procedure as set out in Eurocode 2,<sup>60</sup> the total applied load (Table 4), and the test set-up (Figure 7). Since this calculation was made under serviceability

TABLE 5 Theoretical cracking and failure loads.

Property	12 × 24 × 180-cm beam <sup>a</sup>	24 × 24 × 130-cm beam <sup>b</sup>
Bending-cracking load $LM_{cr}$ (N)	13,067	25,067
Bending-failure load $LM_{ft}$ (N)	32,000	47,580
Shear-failure load $LV_{ft}$ (N)	47,175	54,600

<sup>a</sup>Values calculated according to the set-up of the bending test (Figure 4a) and shear test (Figure 6a).

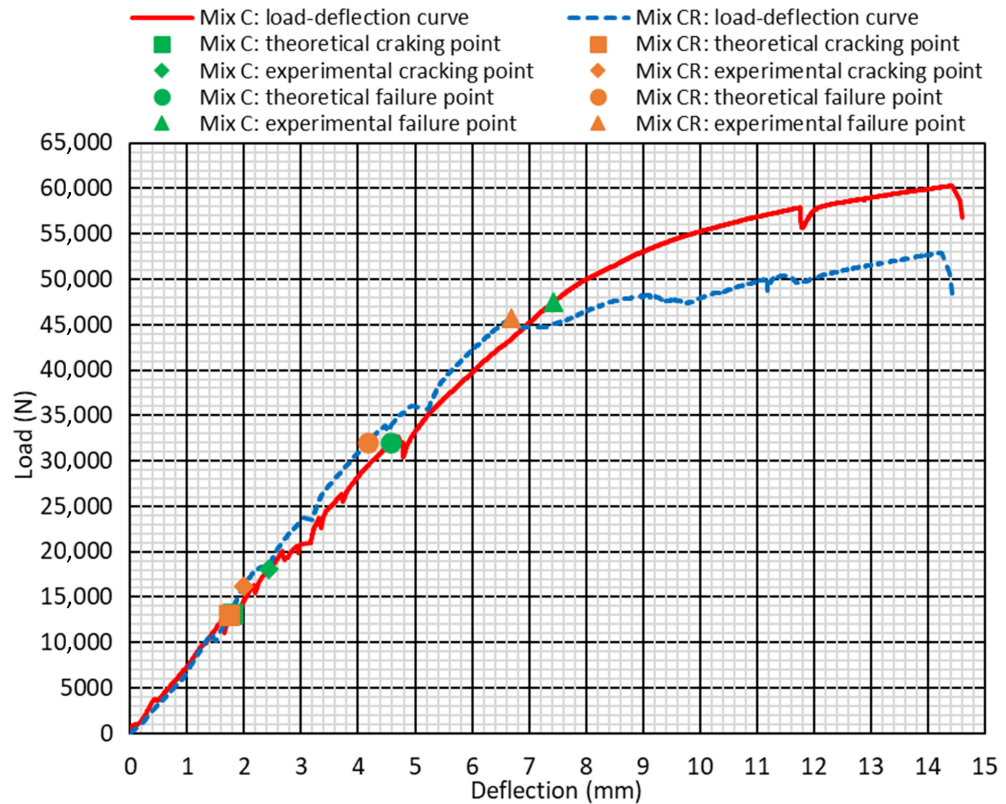
<sup>b</sup>Values calculated as per the set-up of the shear-bending test (Figure 5a).

conditions, unitary safety coefficients were not considered. This curve is detailed in the results section of that test.

## 4 | BEAM TESTING: EXPERIMENTAL RESULTS AND DISCUSSION

Having defined the key theoretical points for the structural tests on the beams in the previous section, the results of those tests are presented in this section. The experimental failure points were defined as those from which the beams began to show plastic performance, thus ensuring that the experimental and theoretical failure points to be compared always corresponded to an elastic-regime behavior. The results of each test are shown below as the average values obtained for the three beams tested for each mix. Moreover, as both SCC mixes

FIGURE 9 Bending test.



under study showed almost the same compressive strength (Table 3), the effect of coarse RA on the structural behavior of the concrete beams in the tests where the behaviors of both SCC mixes were compared (bending and shear-bending test) could be analyzed when RA addition had no effect on concrete strength. This approach differed from the evaluations found in other studies in the literature<sup>32,53</sup> where the structural behavior was evaluated in concrete mixes containing RA of lower strength than those made with 100% NA.

#### 4.1 | Bending test

The bending test was conducted on beams manufactured with both mixes, *C* and *CR*, and the average load-deflection curves are shown in Figure 9. The most characteristic points on these curves are also highlighted, whose load and deflection values are detailed in Table 6 together with the magnitudes that were verified with the required specifications of the precast-concrete company.

The use of coarse RA usually decreases the elastic stiffness of SCC.<sup>64</sup> From the standpoint of structural reinforced concrete, the result is that at the same applied load, the beams containing 100% coarse RA showed higher deflection rates than the beams containing 100% NA.<sup>65</sup> However, in this case, the mix design was such that both mixes had almost the same compressive

strength (Table 3). Together with exactly the same set-up of the reinforcements within the beams of both mixes, such similar mix designs meant that the elastic-deflection zones of the tested beams were almost coincident, regardless of which coarse aggregate (RA or NA) was used for their manufacture. Even the *CR*-mix beams (100% coarse RA) were slightly stiffer. These observations showed that the pre-failure structural behavior of conventional SCC can be successfully simulated using 100% coarse RA provided that a proper mix design is performed. However, two notable effects of coarse RA were detected in this elastic zone:

- On the one hand, cracking was reached for a lower load in the *CR*-mix beams (16.2 kN) than in the *C*-mix beams (18.1 kN), despite the fact that the 180-day compressive strength was 2.5 MPa higher in mix *CR*. One of the main characteristics of RA is its poorer adhesion to the cementitious matrix than NA,<sup>22</sup> which led to premature cracking of the structural beams at earlier stages.<sup>32</sup> It resulted in a lower safety margin for mix *CR* with respect to the theoretical bending-cracking load (Table 6) than for mix *C* (experimental-to-theoretical cracking load ratio of 1.38 vs. 1.24). However, in both cases, it was sufficient to guarantee the structural safety of SCC in the opinion of the structural engineers of the precast-concrete company.

TABLE 6 Main results of the bending test.

		Mix C	Mix CR
Theoretical cracking point	Load (N), Table 5	13,067	13,067
	Deflection (mm)	1.79	1.74
Experimental cracking point	Load (N)	18,060 ± 310	16,190 ± 330
	Deflection (mm)	2.44 ± 0.05	1.98 ± 0.04
Theoretical failure point	Load (N), Table 5	32,000	32,000
	Deflection (mm)	4.57	4.16
Experimental failure point	Load (N)	47,510 ± 560	45,680 ± 600
	Deflection (mm)	7.44 ± 0.11	6.69 ± 0.07
Experimental-to-theoretical cracking load ratio		1.38	1.24
Bending warning coefficient (theoretical cracking), Equation (2)		3.64	3.50
Bending warning coefficient (experimental cracking) <sup>a</sup>		2.63	2.82
Bending safety reserve (%), Equation (1)		32.6	29.9

<sup>a</sup>Coefficient calculated as per Equation (2), but considering the experimental bending-cracking load.

- On the other hand, the failure of mix C occurred at a slightly higher load (47.5 kN) than the failure of mix CR (45.7 kN). The difference between these loads was almost the same as between the cracking loads indicated above, which proves that the reduction of the beam section, due to premature cracking, led to higher stresses within the compressed zone of the CR-mix beams under the same load,<sup>66</sup> thus slightly reducing the failure load. A phenomenon that could also be partly due to the lower strength of RA than NA.<sup>18</sup>

Despite the above, the almost identical compressive strengths of both mixes (Table 3) meant that the main difference between them was their post-failure behaviors. So, while the load-deflection curve of mix CR flattened onto a horizontal plane after failure, showing a high-yielding level of concrete, the curve of mix C still showed a notable load-bearing capacity. Although this zone strongly depends on the yielding and hardening of the tensile reinforcement, mix C exhibited a higher strength reserve after the failure point. Thus, the ultimate load of the C-mix beams was therefore 17% higher than the ultimate load of the CR-mix beams, being this point characterized in both cases by concrete crushing. Therefore, in line with other studies,<sup>32,47,65</sup> it can be stated that the structural beams made of SCC with coarse RA were therefore unable to support as high an additional post-failure load as the components produced with SCC containing 100% NA.

Both mixes comfortably met all the structural verifications that the precast-concrete company required (Table 6), that is, a bending warning coefficient higher than 2.5 and a bending safety reserve of over 20%.

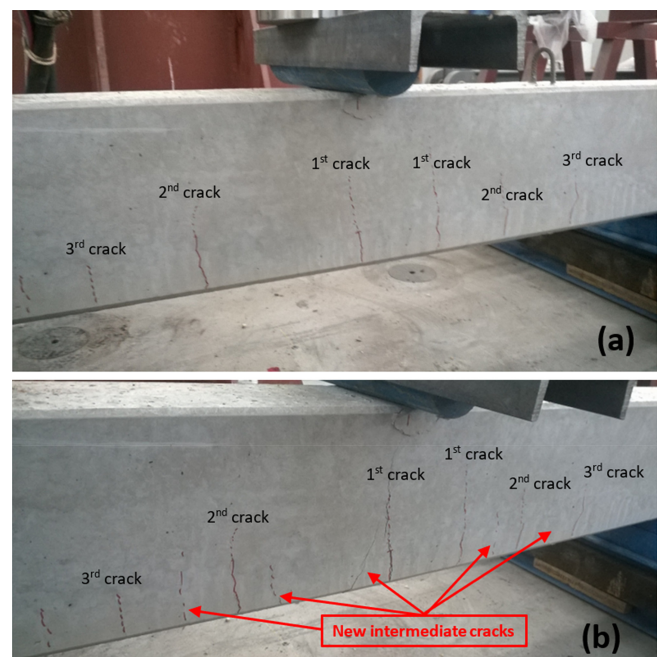
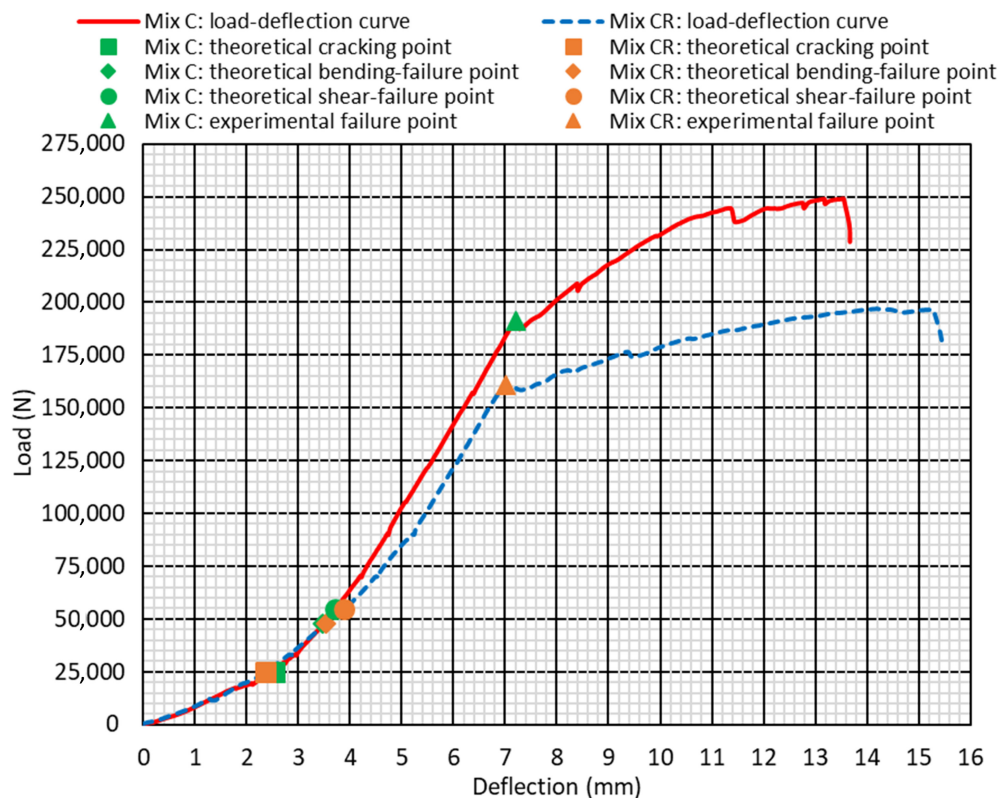


FIGURE 10 Cracking during the bending test of a representative CR-mix beam: (a) theoretical failure point; (b) experimental failure point.

However, as a result of the aspects discussed in this section, these values were slightly better in mix C. Thus, for example, mix C had a safety reserve of 32.6% compared to 29.9% for mix CR. The cracking of mix CR followed the usual patterns,<sup>29,66</sup> with the appearance of vertical bending cracks (Figure 10a) which grew as the load increased at the same time as other intermediate cracks continued to propagate up until failure (Figure 10b). In view of all

FIGURE 11 Shear-bending test.



these aspects, the precast-concrete company was able to affirm that the use of mix *CR* in precast-concrete building components was both feasible and suitable from the point of view of bending stresses.

### 4.2 | Shear-bending test

The shear-bending test of the three beams of each mix, *C* and *CR*, involved the continuous recording of applied load and beam deflection, as well as stoppages to analyze the crack propagation patterns. Figure 11 shows the average deflection curve for both mixes, also showing the most representative points, the values of which are detailed in Table 7.

In the shear-bending test, both mixes showed an elastic behavior up to the failure point, after which the slope of the load-deflection curve decreased sharply, with the beams showing clear yielding. In general terms, the shape of the curve was similar to the obtained in the bending test, although important performance differences were found:

- First, unlike in the bending test, the elastic behavior of the beams in the shear-bending test could be divided into two zones with different slopes. The inflection point of the slope was approximately between the theoretical cracking point and the theoretical bending- and

shear-failure points. Up to this change of slope, the load-deflection curves of both mixes were coincident, which shows that in the zone of the load-deflection curve previous to the theoretical failure points, which are the ones considered in the design, an SCC mix containing 100% coarse RA can show the same structural response as a mix made with conventional NA if both mixes have similar compressive strengths.

- In the second elastic-behavior zone, after the theoretical failure points and up to the experimental failure point, the beams of both mixtures presented similar stiffness, but mix *C* showed a lower deflection for the same load. Unlike the result reported in the previous section regarding the bending test, it was more in line with the literature, according to which the use of coarse RA increases the deformability of SCC when used in structural applications, due to the greater flexibility of RA in comparison with NA.<sup>47,64,65</sup> Beam deformability in the shear-bending test was higher than in the bending test, due to the shorter span of the beams and their higher longitudinal compression reinforcement,<sup>66</sup> so the deflections at which the cracking and failure points were reached were generally higher.
- Regarding the experimental failure point, mix *C* failed at an average load of 191.1 kN, while the failure of mix *CR* occurred at 160.7 kN, which was 15.9% lower. While both mixes failed under similar loading in the

		Mix C	Mix CR
Theoretical cracking point	Load (N), Table 5	25,067	25,067
	Deflection (mm)	2.53	2.36
Theoretical bending-failure point	Load (N), Table 5	47,580	47,580
	Deflection (mm)	3.48	3.54
Theoretical shear-failure point	Load (N), Table 5	54,600	54,600
	Deflection (mm)	3.72	3.89
Experimental failure point	Load (N)	191,070 ± 1400	160,730 ± 1550
	Deflection (mm)	7.21 ± 0.09	7.00 ± 0.10
Bending warning coefficient, Equation (2)		7.62	6.41
Bending safety reserve (%), Equation (1)		75.1	70.4
Shear safety reserve (%), Equation (3)		71.4	66.0

TABLE 7 Main results of the shear-bending test.

bending test, the failure loads in the shear-bending test were very different even though the compressive strengths of both mixes were very similar (Table 3). The interaction between the bending and shear stresses may have favored this behavior,<sup>67</sup> resulting in a worse structural response of the SCC mix containing 100% coarse RA.

- The third and last zone corresponded to the yielding of the concrete in the compressed zone, which occurred immediately after the experimental failure point. As with the bending test, the slope of the load-deflection curve decreased very sharply in both mixes, although they still showed load-bearing capacity. Mix CR demonstrated a similar load-bearing capacity to the one shown in the bending test, following a similar trend to others noted elsewhere.<sup>67,68</sup> Nevertheless, the C-mix beams, as in the bending tests, showed a higher capacity to support loads after failure, possibly due to the higher stiffness of coarse NA compared to RA.<sup>26</sup>

All the structural verifications satisfied the specifications required at the precast-concrete company and the beams were fully compliant, as the values for the bending warning coefficient and the safety reserves were 2–3 times higher than the required values (Table 7). Therefore, the use of mix CR to produce structural precast-concrete elements was, in the opinion of the engineers at the precast-concrete company, feasible from a shear-bending-interaction approach. Furthermore, it should be noted that this wide safety margin was obtained, despite the fact that mix CR (100% coarse RA) performed worse in this shear-bending test than when 100% NA was used, unlike in the bending test where the failure load was practically the same. Finally, it should be emphasized that the cracking of the beams underlined the interaction between bending and shear stresses, as shown in Figure 12. Thus, the first cracks detected were bending

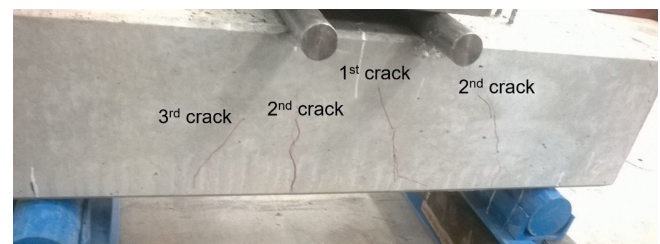


FIGURE 12 Cracking at an intermediate point of the shear-bending test of a CR-mix beam.

cracks (first and second cracks in Figure 12), but later oblique cracks appeared, due to shear stresses (third crack in Figure 12).

### 4.3 | Shear test

The encouraging bending and shear-bending test results led to the decision, in conjunction with the precast-concrete company, to perform the shear test on three CR-mix (100% coarse RA) beams. As with the other failure tests, the applied load and piston displacement were continuously recorded, obtaining the load-deflection curve shown in Figure 14. In addition, the most representative points are depicted, whose values are shown in Table 8.

The load-deflection curve of the shear test and the shear-bending test were both very similar (Figure 13), as both were clearly influenced by the shear stress.<sup>69</sup> Therefore, the same zones were observed in this curve as those described for the other test:

- The initial elastic performance had two zones with different slopes: a first zone with a smaller slope and another in which the beam showed greater stiffness. The initial zone had a lower extension than in the

FIGURE 13 Shear test.

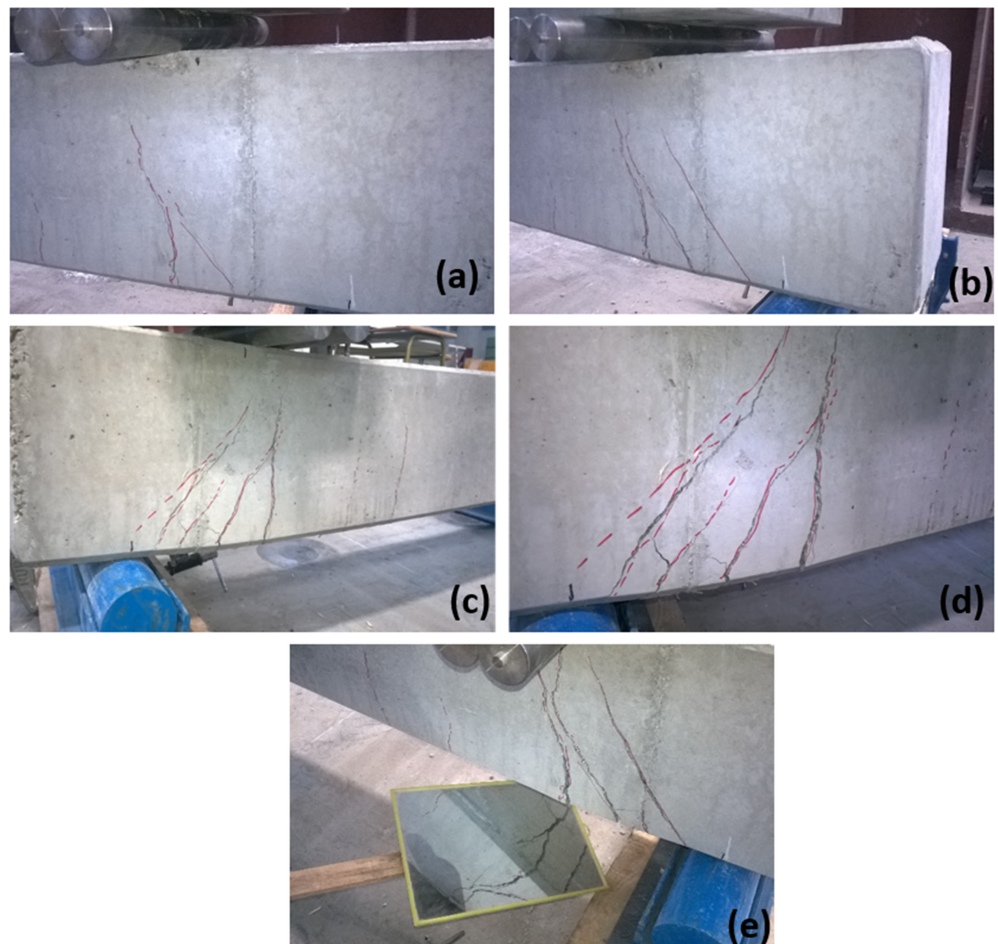
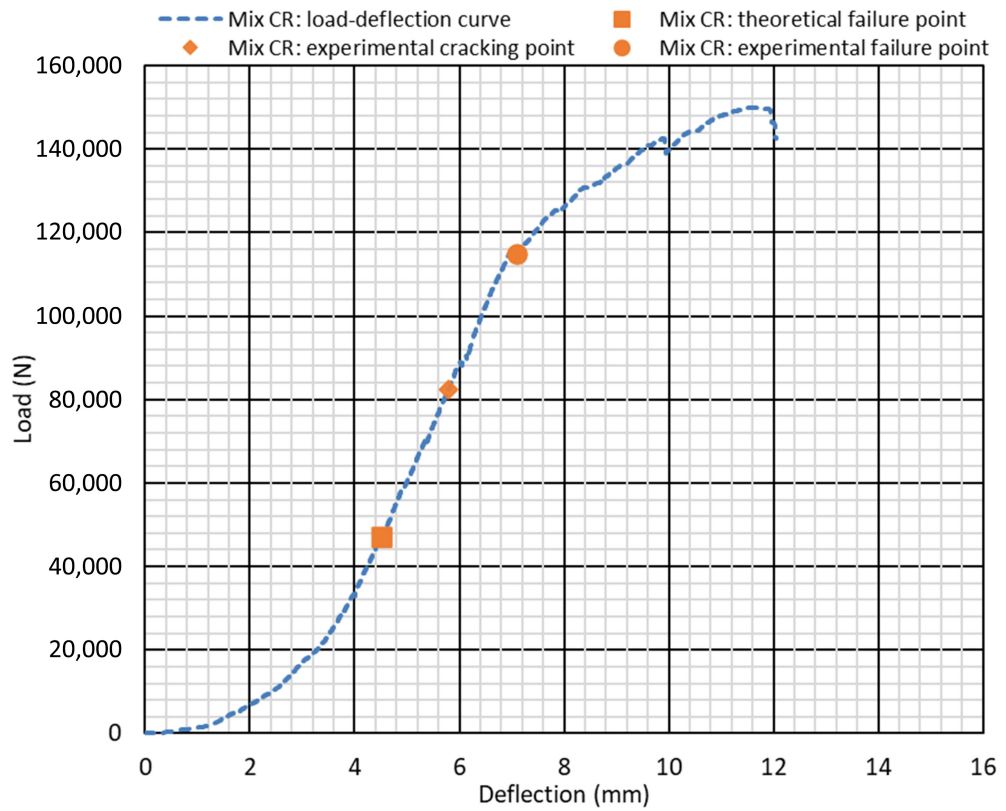


FIGURE 14 Cracking of a CR-mix beam during the shear test: (a) experimental cracking point; (b) experimental failure point; (c) intermediate point after the experimental failure point; (d) experimental ultimate yield point at the end of the test; (e) view of cracking on the lower face of the beam at the ultimate yield point.

shear-bending test, possibly due to the absence of a significant bending moment.<sup>67</sup>

- The second linear elastic zone started at a deflection of approximately 4 mm. The theoretical failure point was located at this zone, at a deflection of 4.52 mm. After this point, the load continued to increase in proportion with the deflection, reaching cracking for a load of 82.5 kN (deflection of 5.80 mm), which was clearly caused by shear stress, as detailed in Figure 14a. It can be noted that the theoretical failure load was around half of the one that caused the first cracking of the beam, which provides initial evidence of the good structural shear behavior of mix CR, as the shear safety reserve was at this point already 42.8% (Table 8). After the experimental cracking point, the load continued to increase in proportion with the deflection up until the experimental failure point.
- The experimental failure load was 115.0 kN (deflection of 7.09 mm), approximately 2.5 times higher than the theoretical failure load, which yielded a shear safety reserve of 59.0%. The safety reserve far exceeded the minimum value required by the precast-concrete company, which showed the validity of mix CR for the precast-concrete industry in terms of withstanding shear stress. The cracking at this point is shown in Figure 14b. The failure results were similar to others reported in the literature.<sup>32,45,65</sup>
- After the experimental failure point, the load-deflection curve was not horizontal, but the beams still showed load-bearing capacity. Thus, cracking continued to increase (Figure 14c) up until failure (load of 149.7 kN, deflection of 11.47 mm). The cracking at this point was very significant, with a crack opening in the order of 4–5 mm (Figure 14d and Figure 14e), which is related to the higher ductility of SCC compared to conventional vibrated concrete, due to its higher cement-paste proportion.<sup>70</sup>

#### 4.4 | Long-term-deflection test

The failure tests were complemented with a serviceability test, the long-term-deflection test. In this way, all structural tests to ensure the applicability of mix CR in the precast-concrete components were covered. As with the shear test, the long-term deflection test was only performed on three CR-mix beams, comparing the theoretically expected and the experimental results.

The average beam deflections at their span midpoints, measured using LVDTs throughout the test, are shown in Figure 15a. The test was performed in a controlled laboratory environment, so that the influence of temperature

TABLE 8 Main results of the shear test.

		Mix CR
Theoretical failure point	Load (N), Table 5	47,175
	Deflection (mm)	4.52
Experimental cracking point	Load (N)	82,460 ± 780
	Deflection (mm)	5.80 ± 0.06
Experimental failure point	Load (N)	114,970 ± 1010
	Deflection (mm)	7.09 ± 0.09
Shear safety reserve (%) as per Equation (3)		59.0
Shear safety reserve (%) regarding cracking point <sup>a</sup>		42.8

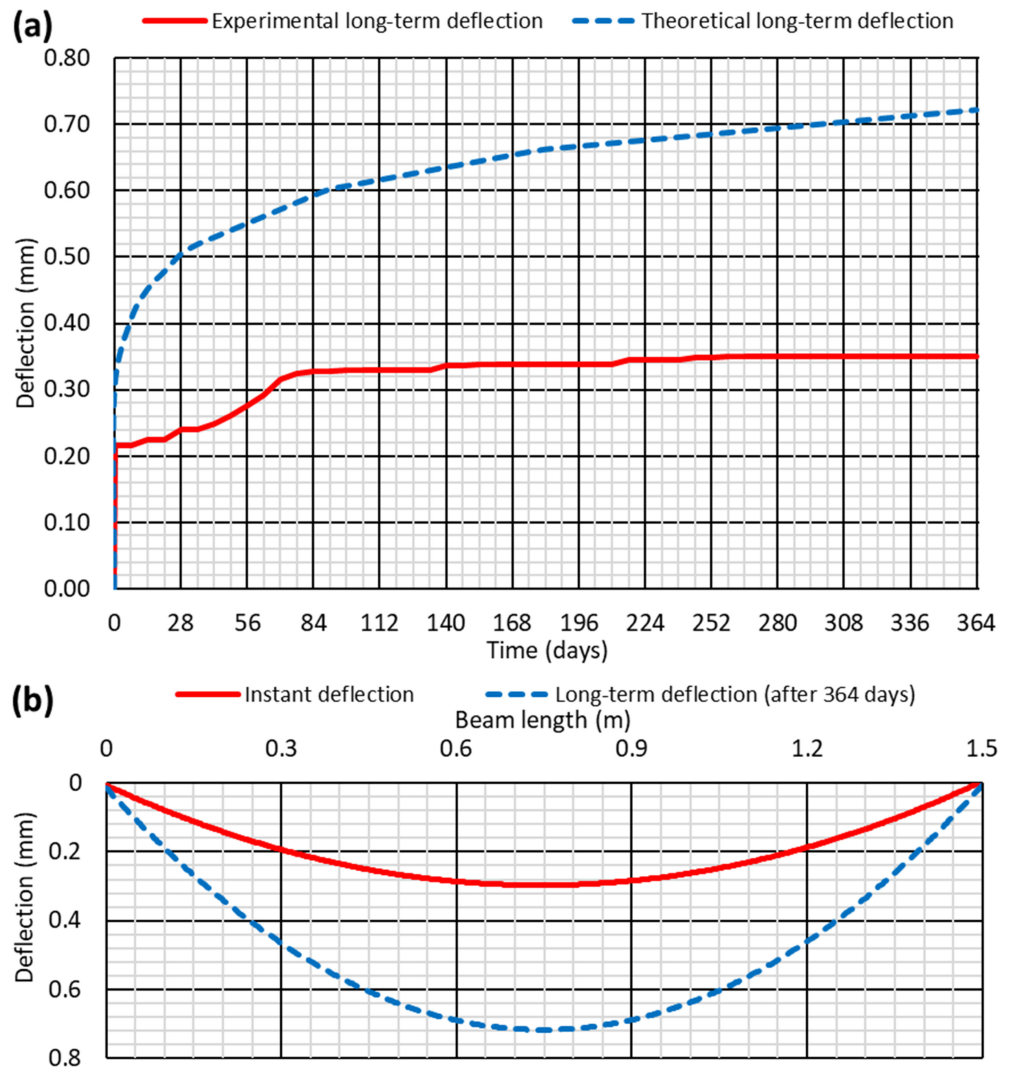
<sup>a</sup>Safety reserve calculated with Equation (3), but considering the experimental cracking load instead of the experimental failure load.

on the results was negligible,<sup>30</sup> and the following relevant points were noted:

- At the point of initial loading, there was a sudden increase in deflection, instant deflection, with a value of 0.216 mm. From that point onwards, the deflection increased slowly over time due to creep phenomena in the concrete and reinforcing bars.<sup>30</sup>
- After the instant deflection, the deflection increased slowly over time, at a rate of 0.0008 mm/day, up until approximately day 42, at which time the deflection began to increase at a rate of around 0.0026 mm/day until day 77. This zone of the long-term-deflection curve had a similar shape to the elastic-behavior zone of the shear-bending and shear tests, which can be explained by the sustained loading of the beams over time.<sup>67</sup>
- As from day 77, the evolution of deflection over time stabilized, increasing at a rate of 0.00014 mm/day until day 259, at which point deflection remained constant and equal to 0.351 mm until the end of the test.

The experimental values were compared with the expected theoretical ones. So, the instant and long-term deflections were calculated according to the formulas of materials resistance (instant deflection) and the Eurocode 2<sup>60</sup> specifications (long-term deflection). No unitary safety coefficient was considered as it was a calculation under serviceability conditions. Thus, Figure 15a shows the theoretical evolution over time of the deflection at the midpoint of the beams, which presented a markedly logarithmic evolution. On the other hand, Figure 15b shows the theoretical instant and long-term deflections (at the end of the test, after 364 days of loading) at all points of the beam. The instant and long-term theoretical deflections at the

**FIGURE 15** Long-term deflection test: (a) deflection evolution over time; (b) theoretical deflection along the beam at the initial and final points of the test.



midpoint of the beam span were 0.301 and 0.722 mm, respectively. Considering that both the instant and the long-term experimental deflections were 0.216 and 0.351 mm, the experimental values represented 71.8% and 48.6% of the theoretical instant and long-term deflection values, respectively. Both deflections met the set requirements of the precast-concrete company, which stated that the experimental value should be at most 80% of the theoretical value for instant deflection and 55% of the theoretical value for long-term deflection. However, it should be noted that, among all the verifications linked to the four tests, the deflection values were the ones that complied with the lowest safety margin, especially in the long term. These results reinforce the idea that serviceability conditions should always be considered in the design of RA-reinforced concrete components, as reported in the existing literature,<sup>32,40,70</sup> and that this aspect also has to be considered in the use of SCC in the precast-concrete industry.

## 5 | CONCLUSIONS

In this study, an experimental campaign conducted with the participation of a precast-concrete company has been reported. The objective has been to verify the structural viability of precast-concrete components made from SCC containing 100% coarse RA. For this purpose, an SCC mix with 100% coarse RA was designed, with which scaled beams were produced following the specifications that are generally required at the company. The beams were subjected to bending, shear-bending, shear, and long-term-deflection tests. The study was complemented with the comparison of the behavior of this mix in the bending and shear-bending tests with the behavior of an SCC mix containing 100% NA of the same compressive strength. The following conclusions can be drawn from the study:

- Both the beams produced with coarse NA and those prepared with coarse RA showed the same stiffness

within the elastic-behavior zone, before the failure point, during the bending and shear-bending tests. Despite the higher flexibility of RA compared to NA, an adequate adjustment of the SCC dosage in terms of water content and superplasticizing admixture meant that the fresh and mechanical behavior of SCC with RA could be balanced, so that the structural behavior of the SCC with 100% coarse NA (0% coarse RA) could be replicated with RA. However, despite the same compressive strength of the mixes, the load-bearing capacity after failure was lower after coarse RA had been added.

- The SCC beams with 100% coarse RA widely complied with all the set requirements at the precast-concrete plant for the failure tests, that is, bending, shear-bending, and shear tests. In fact, the safety checks performed were 1.5–3 times higher than the set requirements. Thus, from a failure-design approach and according to the indications of the collaborating company, the use of SCC with 100% coarse RA would be suitable for producing precast-concrete building elements.
- In relation to in-service conditions, the SCC with 100% coarse RA fulfilled the requirements of the long-term-deflection test within a narrow margin. More specifically, the instant and long-term (after 1 year of loading) experimental deflections were required to be at most 80% and 55% of the theoretical values, respectively. The instant deflection was found to be 71.8% of the theoretical value, while the long-term deflection was 48.6%. These results showed that the design in service was more restrictive than under failure conditions, so the serviceability conditions should always be considered in the design of precast-concrete components of this sort containing maximum proportions of RA.

In general, it may be noted that SCC with 100% coarse RA can be safely used for the manufacture of precast-concrete building elements, although the design should always be based on the serviceability performance, as serviceability is the most restrictive aspect when this alternative aggregate is used in SCC. Nevertheless, these points have been evaluated on scaled beams, so it might be interesting in a subsequent step of the research to study the behavior of real precast-concrete building elements such as delta and slab beams.

## ACKNOWLEDGMENTS

This research work was supported by the Spanish Ministry of Universities, MICINN, AEI, EU, ERDF, and NextGenerationEU/PRTR (grant numbers PID2020-113837RB-I00; doi:10.13039/501100011033; TED2021-129715B-I00; FPU17/03374); the Junta de Castilla y León (Regional Government) and ERDF (grant number UIC-231); and, finally, the University of Burgos (grant number SUCONS, Y135.GI). Finally, the

support and assistance of ARTEPREF S.A. for the development of this study is also highly appreciated and valued.

## CONFLICT OF INTEREST STATEMENT

The authors declare that there is no conflict of interest.

## DATA AVAILABILITY STATEMENT

The data that support the findings of this study are available on request from the corresponding author. The data are not publicly available due to privacy or ethical restrictions.

## ORCID

Francisco Fiol  <https://orcid.org/0000-0002-7388-2839>

Victor Revilla-Cuesta  <https://orcid.org/0000-0003-3337-6250>

Marta Skaf  <https://orcid.org/0000-0001-7205-2692>

Carlos Thomas  <https://orcid.org/0000-0002-2641-9411>

Juan M. Manso  <https://orcid.org/0000-0003-4964-5128>

## REFERENCES

1. Calvo Robledo A, MacDonald MA, Butt C. Restoration scenario planning at a Spanish quarry can be informed by assessing ecosystem services. *Restor Ecol.* 2020;28(4):1006–13.
2. Dias AB, Pacheco JN, Silvestre JD, Martins IM, de Brito J. Environmental and economic life cycle assessment of recycled coarse aggregates: a Portuguese case study. *Materials.* 2021;14(18):5452.
3. Zhao D, Zhang D, Shen W, Huang J, Tang X, Yang Y, et al. Investigation on industrial trial production of multi-phased clinker with crude granular steel slag. *J Clean Prod.* 2022;337:130467.
4. Vavřková MD, Maxianová A, Winkler J, Adamcová D, Podlasek A. Environmental consequences and the role of illegal waste dumps and their impact on land degradation. *Land Use Policy.* 2019;89:104234.
5. Lederer J, Gassner A, Kleemann F, Fellner J. Potentials for a circular economy of mineral construction materials and demolition waste in urban areas: a case study from Vienna. *Resour Conserv Recycl.* 2020;161:104942.
6. Filazi A, Demir İ, Sevim O. Enhancement on mechanical and durability performances of binary cementitious systems by optimizing particle size distribution of fly ash. *Arch Civ Mech Eng.* 2020;20(2):58.
7. Saluja S, Kaur K, Goyal S, Bhattacharjee B. Long-term drying shrinkage of GGBFS-incorporated RCC under various temperature exposures. *J Mater Civ Eng.* 2021;33(6):04021122.
8. Zhang L, Geng T, Liu Z, Zhang W, Shang Q. Effect of silica fume and calcium carbonate whisker on interfacial behavior of near-surface-mounted FRP with magnesium phosphate cement. *Arch Civ Mech Eng.* 2020;20(1):2.
9. Beaucour AL, Pliya P, Faleschini F, Njinwoua R, Pellegrino C, Noumowé A. Influence of elevated temperature on properties of radiation shielding concrete with electric arc furnace slag as coarse aggregate. *Construct Build Mater.* 2020;256:119385.
10. Yu Y, Jin Z, Zhu H, Song H. Effect of rubber particles on impact resistance of concrete at a temperature of  $-20^{\circ}\text{C}$ . *Arch Civ Mech Eng.* 2021;21(3):107.

11. Zheng Y, Zhang Y, Zhang P. Methods for improving the durability of recycled aggregate concrete: a review. *J Mater Res Technol.* 2021;15:6367–86.
12. Zhang B, Ahmad W, Ahmad A, Aslam F, Joyklad P. A scientometric analysis approach to analyze the present research on recycled aggregate concrete. *J Build Eng.* 2022;46:103679.
13. Xu J, Liu Y, Simi A, Zhang J. Recycling and reuse of construction and demolition waste: from the perspective of national natural science foundation-supported research and research-driven application. *Case Stud Constr Mater.* 2022;16:e00876.
14. Mahmood W, Khan AUR, Ayub T. Carbonation resistance in ordinary Portland cement concrete with and without recycled coarse aggregate in natural and simulated environment. *Sustainability.* 2022;14(1):437.
15. Sainz-Aja JA, Carrascal IA, Polanco JA, Thomas C. Effect of temperature on fatigue behaviour of self-compacting recycled aggregate concrete. *Cem Concr Compos.* 2022;125:104309.
16. Paula Junior AC, Jacinto C, Oliveira TM, Polisseni AE, Brum FM, Teixeira ER, et al. Characterisation and life cycle assessment of pervious concrete with recycled concrete aggregates. *Crystals.* 2021;11(2):209.
17. Wu Q, Gong F, Zhi D, Zhao Y. Removing attached mortar from recycled aggregate by the combined freeze–thaw cycles and high-temperature drying. *Struct Concr.* 2022;23(5):3126–39.
18. Martínez-garcía R, Jagadesh P, Búrdalo-salcedo G, Palencia C, Fernández-raga M, Fraile-fernández FJ. Impact of design parameters on the ratio of compressive to split tensile strength of self-compacting concrete with recycled aggregate. *Materials.* 2021;14(13):3480.
19. Chen Y, Li T, Jiang R, Ye P, Cai J. Experimental and damage modeling research on compression-shear behavior of carbon fiber recycled aggregate concrete. *Struct Concr.* 2023;24(1):1471–85.
20. González-Fonteboia B, Seara-Paz S, De Brito J, González-Taboada I, Martínez-Abella F, Vasco-Silva R. Recycled concrete with coarse recycled aggregate. An Overview and Analysis *Mater Constr.* 2018;68(330):e151.
21. Fiol F, Thomas C, Muñoz C, Ortega-López V, Manso JM. The influence of recycled aggregates from precast elements on the mechanical properties of structural self-compacting concrete. *Construct Build Mater.* 2018;182:309–23.
22. Gonzalez-Corominas A, Etxeberria M, Poon CS. Influence of the quality of recycled aggregates on the mechanical and durability properties of high performance concrete. *Waste Biomass Valor.* 2017;8(5):1421–32.
23. Ulsen C, Antoniassi JL, Martins IM, Kahn H. High quality recycled sand from mixed CDW-is that possible? *J Mater Res Technol.* 2021;12:29–42.
24. Bravo M, Duarte APC, Brito JD, Evangelista L, Pedro D. On the development of a technical specification for the use of fine recycled aggregates from construction and demolition waste in concrete production. *Materials.* 2020;13(19):2619.
25. Etxeberria M, Konoiko M, Garcia C, Perez MÁ. Water-washed fine and coarse recycled aggregates for real scale concretes production in Barcelona. *Sustainability.* 2022;14(2):708.
26. Revilla-Cuesta V, Faleschini F, Zanini MA, Skaf M, Ortega-López V. Porosity-based models for estimating the mechanical properties of self-compacting concrete with coarse and fine recycled concrete aggregate. *J Build Eng.* 2021;44:103425.
27. Evangelista L, De Brito J. Durability of crushed fine recycled aggregate concrete assessed by permeability-related properties. *Mag Concr Res.* 2019;71(21):1142–50.
28. Kirthika SK, Singh SK, Chourasia A. Alternative fine aggregates in production of sustainable concrete- a review. *J Clean Prod.* 2020;268:122089.
29. Lanti R, Martínez M. Biaxial bending and axial load in reinforced concrete sections. *Numerical Approach Inf Constr.* 2020;72(558):1–9.
30. Santamaría A, Ortega-López V, Skaf M, Chica JA, Manso JM. The study of properties and behavior of self compacting concrete containing electric arc furnace slag (EAFS) as aggregate. *Ain Shams Eng J.* 2020;11(1):231–43.
31. Faleschini F, Zanini MA, Toska K. Seismic reliability assessment of code-conforming reinforced concrete buildings made with electric arc furnace slag aggregates. *Eng Struct.* 2019;195:324–39.
32. Le HB, Bui QB. Recycled aggregate concretes – a state-of-the-art from the microstructure to the structural performance. *Construct Build Mater.* 2020;257:119522.
33. Anaya P, Rodríguez J, Andrade C, Martín-Pérez B, Hombrados CL. Determination of wires transfer length in prestressed concrete members with different levels of corrosion. *Inf Constr.* 2020;72(558):1–10.
34. Matos JC, Cruz PJS, Valente IB, Neves LC, Moreira VN. An innovative framework for probabilistic-based structural assessment with an application to existing reinforced concrete structures. *Eng Struct.* 2016;111:552–64.
35. Dong H, Song Y, Cao W, Sun W, Zhang J. Flexural bond behavior of reinforced recycled aggregate concrete. *Construct Build Mater.* 2019;213:514–27.
36. Assaad JJ, Matar P, Gergess A. Effect of quality of recycled aggregates on bond strength between concrete and embedded steel reinforcement. *J Sustain Cem Based Mater.* 2020;9(2):94–111.
37. Gao D, Yan H, Fang D, Yang L. Bond strength and prediction model for deformed bar embedded in hybrid fiber reinforced recycled aggregate concrete. *Construct Build Mater.* 2020;265:120337.
38. Pacheco JN, de Brito J, Chastre C, Evangelista L. Bond of recycled coarse aggregate concrete: model uncertainty and reliability-based calibration of design equations. *Eng Struct.* 2021;239:112290.
39. Majhi RK, Nayak AN, Swain RB. Structural performance of RC beams containing high-volume ground granulated blast furnace slag and recycled coarse aggregate with lime. *Construct Build Mater.* 2021;307:124907.
40. Sunayana S, Barai SV. Shear and serviceability reliability of recycled aggregate concrete beams. *ACI Struct J.* 2021;118(2):225–36.
41. Gao D, Zhu W, Fang D, Tang J, Zhu H. Shear behavior analysis and capacity prediction for the steel fiber reinforced concrete beam with recycled fine aggregate and recycled coarse aggregate. *Structure.* 2022;37:44–55.
42. Wang J, Xu Q. The combined effect of load and corrosion on the flexural performance of recycled aggregate concrete beams. *Struct Concr.* 2023;24(1):359–73.
43. Pacheco J, De Brito J, Chastre C, Evangelista L. Uncertainty models of reinforced concrete beams in bending: code comparison and recycled aggregate incorporation. *J Struct Eng.* 2019;145(4):04019013.
44. Pacheco JN, de Brito J, Chastre C, Evangelista L. Uncertainty of shear resistance models: influence of recycled concrete aggregate on beams with and without shear reinforcement. *Eng Struct.* 2020;204:109905.
45. Deresa ST, Xu J, Demartino C, Heo Y, Li Z, Xiao Y. A review of experimental results on structural performance of reinforced

- recycled aggregate concrete beams and columns. *Adv Struct Eng.* 2020;23(15):3351–69.
46. Zhang H, Wu J, Jin F, Zhang C. Effect of corroded stirrups on shear behavior of reinforced recycled aggregate concrete beams strengthened with carbon fiber-reinforced polymer. *Compos Part B Eng.* 2019;161:357–68.
  47. Ghalehnovi M, Karimipour A, Anvari A, de Brito J. Flexural strength enhancement of recycled aggregate concrete beams with steel fibre-reinforced concrete jacket. *Eng Struct.* 2021; 240:112325.
  48. Tang Y, Fang S, Chen J, Ma L, Li L, Wu X. Axial compression behavior of recycled-aggregate-concrete-filled GFRP-steel composite tube columns. *Eng Struct.* 2020;216:110676.
  49. Jiménez R. Study of the validity of the constructive system LAD-MA for the self-help housing of incremental housing. *Inf Constr.* 2020;72(560):1–11.
  50. Fiol F, Thomas C, Manso JM, López I. Transport mechanisms as indicators of the durability of precast recycled concrete. *Construct Build Mater.* 2021;269:121263.
  51. Santamaría A, González JJ, Losáñez MM, Skaf M, Ortega-López V. The design of self-compacting structural mortar containing steelmaking slags as aggregate. *Cem Concr Compos.* 2020;111:103627.
  52. Singh A, Duan Z, Xiao J, Liu Q. Incorporating recycled aggregates in self-compacting concrete: a review. *J Sustain Cem Based Mater.* 2020;9(3):165–89.
  53. Revilla-Cuesta V, Skaf M, Faleschini F, Manso JM, Ortega-López V. Self-compacting concrete manufactured with recycled concrete aggregate: an overview. *J Clean Prod.* 2020;262:121362.
  54. EN-Euronorm, Rue de stassart, 36 Belgium-1050 Brussels, European Committee for Standardization.
  55. Grabiec AM, Kim J, Ubysz A, Bilbao P. Some remarks towards a better understanding of the use of concrete recycled aggregate: a review. *Sustainability.* 2021;13(23):13336.
  56. Güneysi E, Gesoğlu M, Algin Z, Yazici H. Effect of surface treatment methods on the properties of self-compacting concrete with recycled aggregates. *Construct Build Mater.* 2014;64: 172–83.
  57. Carro-López D, González-Fonteboa B, De Brito J, Martínez-Abella F, González-Taboada I, Silva P. Study of the rheology of self-compacting concrete with fine recycled concrete aggregates. *Construct Build Mater.* 2015;96(491–501):7102–501.
  58. Huang H, Yuan Y, Zhang W, Zhu L. Experimental study on the mechanical properties and the microstructure of hybrid-fiber-reinforced concrete under an early stage. *Struct Concr.* 2020;21(3):1106–22.
  59. UNE 36068. Ribbed bars of weldable steel for the reinforcement of concrete. 2011.
  60. EC 2. Eurocode 2: design of concrete structures. Part 1–1: general rules and rules for buildings. CEN (European Committee for Standardization); 2010.
  61. AFNOR. *Encyclopedia du Batiment.* 1992–2010.
  62. Galkovski T, Mata-Falcón J, Kaufmann W. Effective reinforcement ratio of RC beams: validation of modelling assumptions with high-resolution strain data. *Struct Concr.* 2022;23(3): 1353–69.
  63. Löschmann J, Mark P. Strengthening of beams or slabs using temperature induction. *Struct Concr.* 2022;23(5):2770–85.
  64. Silva RV, De Brito J, Dhir RK. Establishing a relationship between modulus of elasticity and compressive strength of recycled aggregate concrete. *J Clean Prod.* 2016;112:2171–86.
  65. Velay-Lizancos M, Vazquez-Burgo P, Restrepo D, Martínez-Lage I. Effect of fine and coarse recycled concrete aggregate on the mechanical behavior of precast reinforced beams: comparison of FE simulations, theoretical, and experimental results on real scale beams. *Construct Build Mater.* 2018;191:1109–19.
  66. Santamaría A, García-Llona A, Revilla-Cuesta V, Piñero I, Ortega-López V. Bending tests on building beams containing electric arc furnace slag and alternative binders and manufactured with energy-saving placement techniques. *Structure.* 2021;32:1921–33.
  67. Yu Z, Shan D. Experimental and numerical studies of T-shaped reinforced concrete members subjected to combined compression-bending-shear-torsion. *Adv Struct Eng.* 2021;24(12):2809–25.
  68. Völgyi I, Windisch A. Experimental investigation of the role of aggregate interlock in the shear resistance of reinforced concrete beams. *Struct Concr.* 2017;18(5):792–800.
  69. Romera JM, Marcos I, Skaf M, Ortega-López V. An alternative experimental methodology to determine the diagonal cracking resistance of steel-reinforced concrete beams. *Eng Struct.* 2021; 244:112741.
  70. Revilla-Cuesta V, Skaf M, Santamaría A, Ortega-López V, Manso JM. Assessment of longitudinal and transversal plastic behavior of recycled aggregate self-compacting concrete: a two-way study. *Construct Build Mater.* 2021;292:123426.

## AUTHOR BIOGRAPHIES



**Francisco Fiol** Department of Construction, Escuela Politécnica Superior, University of Burgos, c/ Villadiego s/n, 09001 Burgos, Spain. [ffiol@ubu.es](mailto:ffiol@ubu.es)



**Víctor Revilla-Cuesta** Department of Civil Engineering, Escuela Politécnica Superior, University of Burgos, c/ Villadiego s/n, 09001 Burgos, Spain. [vrevilla@ubu.es](mailto:vrevilla@ubu.es)



**Marta Skaf** Department of Construction, Escuela Politécnica Superior, University of Burgos, c/ Villadiego s/n, 09001 Burgos, Spain. [mksaf@ubu.es](mailto:mksaf@ubu.es)



**Carlos Thomas** LADICIM (Laboratory of Materials Science and Engineering), E.T.S. de Ingenieros de Caminos, Canales y Puertos, University of Cantabria, Av./ Los Castros 44, 39005 Santander, Spain. [carlos.thomas@unican.es](mailto:carlos.thomas@unican.es)



**Juan M. Manso** Department of Civil Engineering, Escuela Politécnica Superior, University of Burgos, c/ Villadiego s/n, 09001 Burgos, Spain. [jmmanso@ubu.es](mailto:jmmanso@ubu.es)

**How to cite this article:** Fiol F, Revilla-Cuesta V, Skaf M, Thomas C, Manso JM. Scaled concrete beams containing maximum levels of coarse recycled aggregate: Structural verifications for precast-concrete building applications. *Structural Concrete*. 2023;24(3):3476–97. <https://doi.org/10.1002/suco.202200963>